Crystal Research and Technology

REPRINT

WILEY-VCH

X-ray, synchrotron, and neutron diffraction analysis of Roman cavalry parade helmet fragment

Ľ. Smrčok*[1], I. Petrík[2], V. Langer[3], Y. Filinchuk[4], and P. Beran[5]

[1] Institute of Inorganic Chemistry, Slovak Academy of Sciences, Dúbravská cesta 9, 84536 Bratislava, Slovak Republic
[2] Geological Institute, Slovak Academy of Sciences, Dúbravská cesta 9, 84005 Bratislava, Slovak Republic
[3] Environmental Inorganic Chemistry, Chalmers University of Technology, 412 96 Gothenburg, Sweden
[4] Swiss-Norwegian Beam Lines, European Synchrotron Radiation Facility, 6 rue Jules Horowitz, BP-220, 38043 Grenoble CEDEX, France
[5] Nuclear Physics Institute ASCR v.v.i. and Research Centre Řež Ltd., 25068 Řež, Czech Republic

A partially corroded fragment of the neck guard of a Roman cavalry helmet excavated in the former military camp of Gerulata, a part of the Limes Romanus on the River Danube, was analysed by laboratory X-ray, synchrotron and neutron powder diffraction. The approximate phase composition determined by the neutron diffraction of the bulk, 82% (wt) of the copper alloy phase, 12 % (wt) of cuprite and 6% of nantokite indicate a significant degree of corrosion of the artefact. Elemental EDX analysis of cleaned surface showed that the chemical composition of the original alloy is 78 to 82 % (wt) of Cu and 21.4 to 16.5 % of Zn with minute amounts of Sn, Si and S. High contents of Cu and Zn with the negligible amount of Sn showed that the body of the helmet was made of brass and not of bronze as expected before. The amount of zinc in the copper alloy calculated from the refined lattice parameter agrees fairly well with the value determined by EDX. The most abundant phase in the synchrotron powder diffraction pattern of the corrosion products scrapped from the artefact is cuprite, but presence of atacamite, malachite, brochantite, nantokite, mixed Cu-Zn hydroxyl carbonates and probably also of simonkolleite ($Zn_5(OH)_8Cl_2.H_2O$) have been detected. In contrast, the X-ray pattern taken directly from the surface of the artefact is dominated by atacamite with some traces of malachite and quartz. Because the penetration depth of laboratory X-rays is in order of tens of microns, the phase analysis based only on a diffraction pattern taken from a surface can lead to erroneous conclusions concerning the phase composition of the patina.

1   Introduction

In 1979 a Roman helmet was excavated at the site of the former Roman military settlement Gerulata situated to the East of Carnuntum, the capital of the Roman province of Pannonia Superior (Upper Pannonia). The military camp of Gerulata was built in the 2nd century AD as a part of the fortification system along the Northern frontier of the Roman Empire, the Limes Romanus, situated at the right bank of the main flow of the River Danube. The camp was abandoned in the 4th century AD, when the Roman legions withdrew from Pannonia. At the present time the ruins of the camp destroyed in the wars with the German tribes between 166 and 180 AD are located in the suburban area (Rusovce) of the capital of the Slovak Republic, Bratislava.

The richly decorated pseudo-attic cavalry parade helmet of the "Guisborough type" (see e.g. [1] and www.romancoins.info/MilitaryEquipment-Guisborough.html) was found in strongly deformed condition (Fig. 1a) in a layer of collapse debris at a depth of 136 cm [2]. In addition to the compact helmet body several corroded pieces of different sizes evidently detached from the helmet were also unearthed nearby. The largest artefact is a piece of the neck guard, obviously missing from the bottom of the helmet (Fig. 1b). This slightly twisted, compact fragment is approx. 10 cm long and approx. 2.5 cm wide (Fig. 2) and whilst the smaller (5 to 7 mm at maximum) scraps are extensively corroded, the largest piece is covered only by a relatively thin (~200

* Corresponding author: e-mail: uachsmrk@savba.sk

to 300 μm) patina of dark reddish colour. Its surface is relatively rough, containing small areas of turquoise colour crystallites and represents a passive film in steady-state conditions [3].

This work presents the results of the X-ray, synchrotron and neutron diffraction analysis of the largest artefact with the aim of collecting information related to its original composition and to identify the corrosion products. The knowledge obtained will help to improve the typological classification of the Roman military equipment found near the Central European part of the Limes and thus contribute to the investigation of provenance. Identification of corrosion products can shed more light on the mechanism of the corrosion processes of copper alloys and can prove useful for conservation and restoration works of ancient artefacts. The choice of diffraction experiments was motivated by the very different penetration depths of neutron, synchrotron and laboratory X-ray radiation as well as by different resolutions typical for all the three experimental arrangements.

Fig. 1 a) View of the helmet from the back right side. The top of the helmet is not visible as it was forcibly pressed into the interior before the helmet was excavated. The well preserved right cheek can be recognized as well as the slightly bent "strip" of the neck guard in the bottom. b) View from the bottom. The better preserved right cheek is now on the left, while the almost completely corroded piece of the left cheek is on the top. The residue of the neck guard protection is visible at the bottom. Photo courtesy of Dr. Schmidtová (Bratislava City Museum) and Dr. Šimko (Institute of Inorganic Chemistry, Slovak Academy of Sciences, Bratislava). (Online color at www.crt-journal.org)

Fig. 2 The analysed fragment of the neck guard. The brighter strip in the middle is the part with patina removed. The smallest unit is 1 millimeter.
(Online color at www.crt-journal.org)

2   Experimental

Transmission X-ray powder diffraction patterns were collected using Co $K\alpha_1$ radiation with Stoe Stadi P diffractometer equipped with a linear PSD and a curved Ge (111) primary-beam monochromator. The samples were mounted between two Mylar foils. To collect the reflection patterns a Siemens D5000 diffractometer in grazing-incidence geometry (incidence-beam angle fixed at 8°, secondary long Soller slits and Sol'X energy dispersive detector) was used. The compact sample was illuminated with a parallel beam (Cu $K\alpha_{1,2}$) produced by a primary curved Göbel multilayer mirror. The data were collected with $\Delta 2\theta = 0.05°$ and τ=60 s.

Synchrotron powder diffraction data were collected at the Swiss-Norwegian Beam Lines at the ESRF (Grenoble, France) with a powder sample filled into a 0.5-mm diameter glass capillary. The data collections were performed at the RT using the monochromatic wavelength of $\lambda = 0.720852$ Å with a MAR345 image plate detector. Three sample-to-detector distances (150, 250 and 350 mm) were used in order to combine the advantages of the high structural and angular resolution. The detector parameters and the wavelength were calibrated with a standard sample of LaB_6 produced by the NIST. The capillary was rotated by 60° during 60 seconds of the exposure. The uncertainties in the integrated intensities obtained by integration of the two-dimensional data with the Fit2D program [4] were calculated at every 2θ point by applying Poisson statistics to the intensity data and considering the geometry of the detector [5].

Neutron powder diffraction data were recorded using the instrument MEREDIT (http://neutron.ujf.cas.cz/meredit) in the Nuclear Physics Institute at Řež near Prague, Czech Republic. The neutron beam was monochromatized using a mosaic copper (220) monochromator. The value of the wavelength refined to 1.46 Å using a SiO_2 powder sample. Small contamination of the secondary beam by $\lambda/2$

radiation (~0.4%) was not considered in the data analysis. Diffraction data were collected under the following conditions: 4-148°/0.05° 2θ/350 s. To improve the counting statistics the data were collected in two subsequent runs and the overlapped data were averaged. The 2×4 cm^2 beam was centred approximately to the middle of the slab-shaped sample oriented so as to maximize the irradiated area.

All calculations were done using the FULLPROF2000 [6] and WINPLOTR [7] programs. Both the Le Bail strategy and the refinements with the atomic parameters fixed were applied at the different stages of the data analysis, utilizing the structural data of copper [8] (*Fm*-3*m*, PDF 04-0836) atacamite [9] (Cu$_2$Cl(OH)$_3$, *Pnma*, PDF 25-0269), nantokite [10] (CuCl, *F*-43*m*, PDF 82-2114) and cuprite [11] (Cu$_2$O, *Pn*-3*m*, PDF 05-667). In all the refinements typically only a few selected profile parameters were varied – the scale factors, full width at the half maximum (FWHM) parameters of either modified Lorentzian (X-ray data) or Gaussian (neutron data) profile functions, the overall displacement parameters Q [Å^2] and the unit cell parameters. The angular variations of the backgrounds were approximated in advance by linear interpolation and not further refined.

Local chemical composition was determined by energy dispersive X-ray analysis (EDX) using a SEM JEOL 5800 microscope equipped with a vacuum chamber sufficiently large to accommodate a ca 10 cm long sample. Acceleration voltage was set at 30 kV, sample current was 90 nA. All scanned areas were of ~1500 x 1500 μm^2 size, so that they covered a sufficiently large area to get the representative chemical compositions of the selected surfaces. The analysis provided standardized ZAF corrected data using the following standards: quartz (Si, O), pyrite (S), wollastonite (Ca), and oxides for Mg, Al, metal Cu, Zn and Sn, as well as KCl (Cl), CaCO$_3$ (C). The results were normalized to 100%.

3   Results and discussion

Phase analysis of the bulk   The first information on the phase composition of the bulk was obtained by the neutron powder diffraction. Qualitative phase analysis revealed that the most abundant phases are a cubic copper alloy phase and cuprite (Fig. 3). The refined lattice parameter of the copper alloy phase (3.6574(1) Å) is larger than that expected for the pure copper (3.6145 Å) indicating a certain degree of substitution by a metal with a larger atomic radius. Three weak peaks at ~27.0, 44.8 and 53.1° 2θ, which are not explained by the alloy phase and cuprite correspond to the three most intense peaks of nantokite (111, 220, 311). Inclusion of this structure in the calculations has resulted in the following amounts of the phases (wt%): 82 (alloy):12 (cuprite):6 (nantokite). The lattice parameter of cuprite has been refined to 4.2677(7) Å, which is in good agreement with the reference value of 4.2685(5) Å. The accuracy of the refined cell parameter of nantokite, 5.4119(9) Å vs. 5.4202(2) Å is understandably lower, considering the number of its peaks which are in the pattern above the background level.

The estimate of the cuprite's share agrees well, for example, with the mean amount of cuprite found by neutron diffraction in the study of various Etruscan bronzes, namely ~18% (wt) [12]. Quite surprisingly, nantokite has been identified only in one quarter of the studied Etruscan artefacts and its amount has not exceeded 2.5%(wt). It is, however, our experience [13] that the accuracy of such small shares estimated by the diffraction methods could be low and so must be taken with care, in particular if the number of contributing diffractions is as small as in our pattern.

To advance with the phase analysis of both the original material and the patina, a narrow band (ca. 1 cm wide) of the patina was scraped by a piece of a sharp quartz glass. Supporting chemical information was obtained by three EDX scans made one on the typical patina area and two on the freshly cleaned metallic core strip. The fresh surface was uneven due to scraping, showed gold metallic colour and contained darker pits of deeper, corroded surface, which were avoided from the analysed areas. The EDX analysis of the strip has shown (Table I) that its chemical composition is 78/82% (wt) Cu and 21.4/16.5% Zn, with the amount of Sn not exceeding 0.7/0.8% and S and Si making less than 1%. The alloy is hence almost a pure brass and not a bronze as stated before [2].

Comparison of the lattice parameter of the alloy phase with the figures found for the modern Cu-Zn alloys [14,15] has given two close estimates of the amount of Zn in the artefact, ~15 and ~18% (wt), respectively. These estimates agree fairly well not only with the values determined by the EDX analysis, but are also consistent with the overall zinc contents (~16%) reported for the majority of Roman brass objects from the 1st century AD [16]. The amount of zinc in brass is known to be clearly related to the respective manufacturing processes developed in the course of the centuries. Although the method used in Romans times, a cementation technique based on high temperature zinc vapour diffusion into the metallic copper [17] allows 32% of Zn in

the alloy at the maximum, the ceiling reached by the Romans in their common practice was ~ 28%. Note however that extreme values are rare and appear only at the very right tail of zinc in Roman copper alloys distribution [16]. The amount of Sn found by our microchemical analysis correlates well with the scatter plot relating Zn and Sn contents presented in the same study. Interestingly, no lead was identified in the alloy, although the Sn vs. Pb scatter plot in Craddock's study suggests ~1% or less of Pb. The mutual agreement of the amounts found by the local EDX analysis and neutron diffraction is also worth noting, although the sampled volumes are extremely different – cubic micrometers (EDX) vs. cubic centimeters (neutrons).
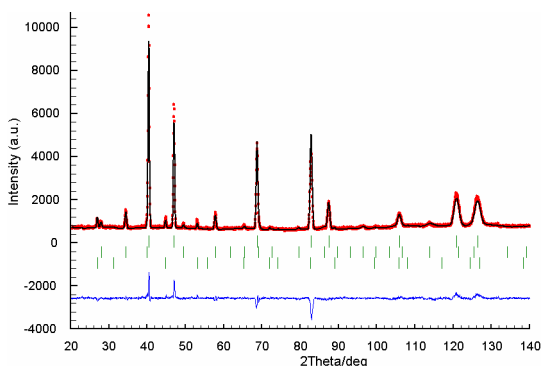

Fig. 3 Neutron Rietveld fit for the bulk sample. The Bragg markers correspond to (from top to bottom) copper alloy, Cu_2O and CuCl, respectively. $R_{wp} = 0.18$, $R_B(alloy) = 0.12$, $R_B(Cu_2O) = 0.18$, $R_B(CuCl) = 0.22$. (Online color at www.crt-journal.org)
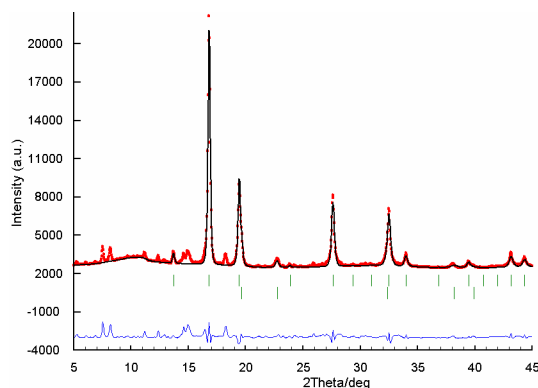
Fig. 4 X-ray synchrotron Rietveld fit for scraped patina powder. The Bragg markers correspond to (from top to bottom) Cu_2O and the copper alloy. $R_{wp} = 0.21$, $R_B(Cu_2O) = 0.15$, $R_B(alloy) = 0.19$. (Online color at www.crt-journal.org)
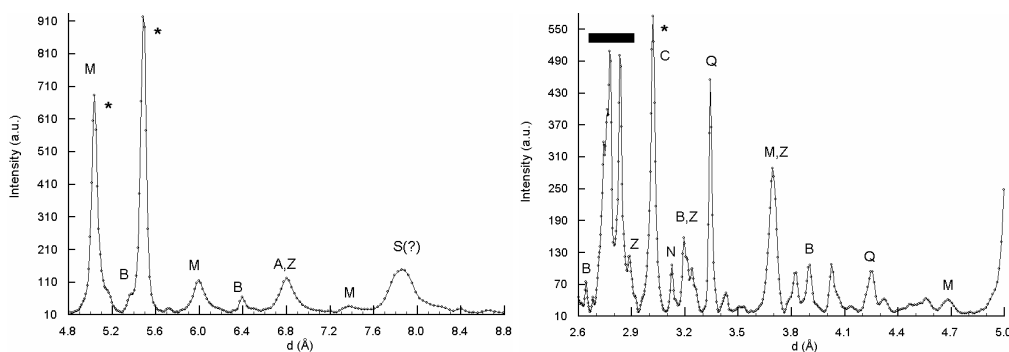

Fig. 5 Low-angle regions of the X-ray synchrotron pattern with the peaks' assignments. Legend: S-Simonkolleite ($Zn_5(OH)_8Cl_2.H_2O$; PDF 77-2311), M-Malachite ($Cu_2(CO_3)(OH)_2$; PDF 41-1390), A-Aurichalcite ($Zn_3Cu_2(OH)_6(CO_3)_2$; PDF 82-1253), B-Brochantite ($Cu_4SO_4(OH)_6$; PDF 43-1458), Q-Quartz (SiO_2,; PDF 86-2237), N-Nantokite (CuCl; PDF 77-2383), Z- Copper Zinc Carbonate Hydroxide (($Cu_xZn_{1-x})_5(CO_3)_2(OH)_6$;PDF 38-0152 for x=0.3, 38-0154 for x=0.2). The atacamite's peaks are labelled with * and cuprite's with C. The band indicated by the thick bar is formed mostly by the diffractions of atacamite.

Phase analysis of the patina powder   Qualitative phase analysis of the scraped powder based on the laboratory X-ray transmission data showed that the prevailing phase is cuprite, but identification of several low-intensity peaks blended with the background was problematic. The analysis therefore continued with the synchrotron X-ray diffraction patterns taken with the better angular resolution and having better signal-to-noise ratio. Better resolution immediately helped us to identify the peaks of the copper alloy phase appearing in the patterns most probably due to too strong scraping (Fig. 4), although the hypothesis on formation of copper crystals by reduction of CuCl could also be considered [18]. The lattice parameter of the alloy phase (3.656(2) Å) has confirmed the value obtained for the neutron data and hence also the estimated composition. Similarly, the refined lattice parameter of cuprite (4.2709(9) Å) is consistent with the value obtained by neutron diffraction, the absolute difference being only 0.0033 Å. The rough estimate of the phase composition

of the scraped powder calculated using just those two phases is then 94% (wt) of cuprite and 6% of the copper alloy phase. Although these two phases have successfully explained the origin of the vast majority of the diffracted intensity, a large number of weak peaks emerging especially in the region of 4 to 16° 2θ (8.8-2.6 Å) remained unassigned (Fig. 5). Unfortunately, this 2θ region is rather narrow and this fact maximizes the risk that phase identification will be based on a rather limited number of diffraction peaks and the results of such a search will be biased. Elimination of unwanted phases in the quest can be partially controlled by application of chemical constraints, but since the chemical composition is in our case determined from a rather small volume compared to the volume of the diffracting powder, it could turn out to be unrepresentative. Secondly, identification of corrosion products (e.g. of mixed salts) could obviously be restricted by the limited amount of the relevant reference patterns in the PDF database.

The local micro-chemical picture of the patina shows that it has fairly complicated composition with the original metals forming only ca. 53% of the total analysis (Table 1). The high percentages of C and O and presence of Cl support the results of the X-ray qualitative phase analysis given in figure 5, since they indicate the presence of the secondary minerals, atacamite and malachite ($Cu_2(CO_3)(OH)_2$). Presence of cuprite and malachite (but not of atacamite) has been documented by X-ray diffraction, for example, in the corrosion products found on a Corinthian-type bronze helmet from the 7th century BC [19]. The most common corrosion products found on the bronze artefacts found in Swedish territory have been cuprite, malachite and basic copper chlorides such as atacamite and paratacamite [20]. All these minerals are reported to have been identified in the corrosion products of bronze Byzantian coins ([21].

Occurrence of the five peaks of the brochantite phase (Fig. 5) implies attack by sulphate ions in the past as no remarkable amount of sulphur was detected by the EDX. This hypothesis is supported by the fact that both brochantite and simonkolleite have been recognized among the corrosion products of a modern brass attacked by artificial and natural sea water simulating chloride and sulphate attack [22]. Simonkolleite has also been identified in the study of brass corrosion in NaCl and $(NH_4)_2SO_4$ during cyclic wet-dry conditions [23]. It should, however, be pointed out that the presence of the rare mineral simonkolleite in our sample is documented only by the presence of its strongest diffraction at $d\sim7.85$ Å, because its second strongest diffraction ($d\sim2.67$ Å) with the relative intensity $I_{rel}\sim25$ falls to the region populated by the diffractions of atacamite. Brochantite was also mentioned among the corrosion products of the artefacts found in very different territories with different corrosion conditions [20,21]. The mechanism of formation of the mixed copper-zinc salts aurichalcite and the chemically related $(Cu_xZn_{1-x})_5(CO_3)_2(OH)_6$ phase is not known to us, but they frequently appear in oxidized zones of copper and zinc deposits. Few diffraction peaks remained that still could not be assigned using the PDF database with the chemistry constraints set according to table 1.

Finally, the elements Ca, Si, Al, K and Fe present in the surface area obviously come from reactions with the soil environment under the presence of underground water supplied mainly by the River Danube.

Table 1 Percentages (wt. %) of the elements determined by EDX at the two points of the cleaned surface ("C") and at one point of the patina ("P").

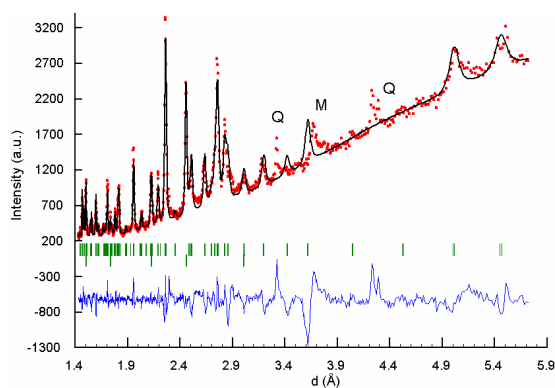| Sample	Cu	O	Sn	Zn	Fe	Si	Al	Ca	Mg	K	Cl	C	S	P
C1	81.7		0.9	16.6		0.6							0.2	
C2	77.9		0.7	21.4										
P	34.8	22.5	0.	17.8	0.8	2.8	0.7	1.3	0.2	0.4	0.6	16.5	1	0.8

Fig. 6 X-ray reflection LeBail fit for the patina on the surface. The Bragg markers correspond to (from top to bottom) atacamite and cuprite.. R_{wp} = 0.28. The diffraction maxima at 3.32, 3.66 and 4.28 Å are assigned to the 101 and 100 diffractions of quartz (Q) and to the 220 diffraction of malachite (M). The linearly increasing background has its origin in the scattering on air, influence of topology of the sample, fluorescence, etc. (Online color at www.crt-journal.org)

Phase analysis of the surface   Because in archaeological and archaeometric practice it is often required to preserve the specimens intact and sampling is therefore not permitted, an attempt was made to estimate the phase composition of the patina also from the laboratory X-ray diffraction pattern taken directly from the surface. Considering the curved and uneven shape of the sample, it was mounted with its outer concave surface in the middle of the diffractometer. Qualitative phase analysis done by the commercial software package EVA © (Bruker AXS, 2008) in combination with the powder diffraction database PDF-4 unambiguously revealed atacamite and cuprite to be the main components, the few small peaks were assigned to the 220 diffraction of malachite and 101 and 100 diffractions of quartz, but nantokite has not been identified (Fig. 6). Splitting of the diffraction band centred at $d{\sim}5.5$ Å implies the presence of a smaller amount of paratacamite, which has its strongest 101 diffraction at $d{=}5.449$ Å (PDF 87-0679). In spite of this successful qualitative phase analysis, the Rietveld fit obtained with the atomic parameters of atacamite and cuprite fixed was, however, not good and the R_{wp} varied between 0.4 and 0.6. Such larger values can most probably be attributed to two facts: i) the experimental data were not taken from a fine powder and non-random orientation of grains can produce false ratios of diffracted intensities, ii) discrepancies between the real structure of the phase developed in a corrosion process and the ideal structure derived from the single crystal data. Relaxation of the structural parameters was however not a remedy, because it led to divergence of the refinements and also to the non-physical values of the isotropic displacement parameters. The results shown in figure 6 thus represent the fit reached using the LeBail strategy and the constant weights assigned to the observed intensities. The lattice parameters of both phases obtained under such unfavourable conditions are unsurprisingly less accurate ($|\Delta a|{=}0.006$ Å, $|\Delta b|{=}$ 0.017 Å and $|\Delta c|{=}$ 0.062 Å for atacamite and $|\Delta a|{=}0.01$ Å for cuprite), but these differences can be, considering the severe conditions for data collection, in many situations acceptable. Note that quartz and malachite were not included in the LeBail fit because their diffractions strongly overlap with those of atacamite.

4   Conclusion

The high contents of Zn and negligible amount of Sn showed that the body of the helmet was made of brass and not of bronze as expected before. The zinc content in the original alloy estimated by neutron diffraction is in accordance with microchemical analysis and with the limits of the cementation technology commonly used by the Romans. Neutron diffraction analysis averaging over a large area of the bulk sample showed that the dominant crystalline corrosion products are cuprite and nantokite in the 2:1 weight ratio. Both these phases have been shown to play crucial roles in the chemical reactions leading to corrosion of the copper alloys [22,24]. The most abundant phase in the synchrotron powder diffraction pattern of the scraped patina is cuprite. A very important result is that the phase composition derived from the X-ray data taken directly from the surface layers remarkably differs from the phase composition of the scrapped powder containing all layers of the patina in one blend. This difference clearly shows that the patina consists of several mineralogically different layers as has been recently documented by SEM-EDX analysis [25]. Because the penetration depth of the X-rays produced by a common X-ray source is in order of tens of microns, phase analysis based on nothing more than a diffraction pattern taken from a surface can lead to erroneous conclusions concerning phase composition and, consequently, also of the character of corrosion processes. The presence of the secondary copper minerals and mixed Cu-Zn salts indicates interaction with a relatively reducing soil environment.

References

[1]   H. R. Robinson, The Armour of Imperial Rome (Arms and Armour Press, London, 1975), p. 200.
[2]   E. Krekovič and L. Snopko, Arch. Korr. **28**, 283 (1998).
[3]   L. Robbiola, J.-M. Blengino, and C. Fiaud, Corr. Sci. **40**, 2083 (1998).
[4]   A. P. Hammersley, S. O. Svensson, M. Hanfland, A. N. Fitch, and D. Häusermann, High Pressure Res. **14**, 235 (1996).
[5]   S. Vogel, L. Ehm, K. Knorr, and G. Braun, Adv. X-ray Anal. **45**, 31 (2002).

[6]   J. Rodriguez-Carvajal, Physica B **192**, 55 (1993).
[7]   T. Roisnel, and J. Rodriguez-Carvajal, Mat. Sci. Forum, **378-381**, 118 (2000).
[8]   W. L. Bragg, Phil. Mag. **28**, 355 (1914).
[9]   J. B. Parise, and B. G. Hyde, Acta Cryst. C **42**, 1277 (1986).
[10]   S. Hull, and D. A. Keen, Phys. Rev. B **50**, 5868 (1994).
[11]   A. Kirfel, and K. Eichhorn, Acta Cryst. A **46**, 271 (1990).
[12]   G. Festa, P. A. Caroppi, A. Filabozzi, C. Andreani, M. L. Arancio, R. Triolo, F. Lo Celso, V. Benfante, and S. Imberti, Meas. Sci. Technol. **19**, 034004 (2008).
[13]   O. Pritula, Ľ. Smrčok, D. M. Többens, and V. Langer, Powder Diffr. **19**, 232 (2004).
[14]   A. Steuwer, P. J. Withers, J. R. Santisteban, L. Edwards, G. Bruno, M. E. Fitzpatrick, M. R. Daymond, M. W. Johnson, and D. Wang, phys. stat. sol. (a) **185**, 221 (2001).
[15]   F. Grazzi, L. Bartoli, S. Siano, and M. Zoppi, Anal. Bioanal. Chem. DOI: 10.1007/s00216-010-3815-4 (2010).
[16]   P. T. Craddock, J. Arch. Sci. **5**, 1 (1978).
[17]   J. Bayley, J. Hist. Metall. Soc. **18**, 42 (1984).
[18]   J. Wang, Ch. Xu, and Ch. Lv, Appl. Surf. Sci. **252**, 6294 (2006).
[19]   E. Pantos, W. Kockelmann, L. C. Chapon, L. Lutterotti, S. L. Bennet, M. J. Tobin, J. W. F. Mosselmans, T. Pradell, N. Salvadó, S. Butí, R. Garner, and A. J. N. W. Prag, Nucl. Instr. Meth. Phys. Res. B **239**, 15 (2005).
[20]   K. Tronner, A. G. Nord, and G. C. Borg, Water Air Soil Poll. **85**, 2725 (2005).
[21]   I. Sandu, N. Ursulescu, I. G. Sandu, O. Bounegru, I. C. A. Sandu, and A. Alexandru, Corr. Eng. Sci. Technol. **43**, 256 (2008).
[22]   C. I. S. Santos, M. H. Mendonça, and I. T. E. Fonseca, J. Appl. Electrochem. **36**, 1353 (2006).
[23]   G. A. El-Mahdy, J. Appl. Electrochem. **35**, 347 (2005).
[24]   D. A. Scott, J. Am. Inst. Conserv. **29**, 193 (1990).
[25]   I. Constantinides, A. Adriaens, and F. Adams, Appl. Surf. Sci. **189**, 90 (2002).